Analysis and Design of Doubly Curved Piezoelectric Strip-Actuated Aperture Antennas

Hwan-Sik Yoon, Gregory Washington, and Wilhelmus Hendrikus Theunissen

***Abstract*—Recently, aperture antennas that have the ability to change their reflector shape through the use of piezoelectric actuators have been studied. The results show that those antennas can exhibit beam steering and beam shaping in the far field. However, many of the previous studies have been confined to cylindrical shape antennas. This study examines the use of "doubly curved" antenna structures to achieve better performance in controlling an antenna's coverage area. The spherical antenna is modeled as a shallow spherical shell with a small hole at the apex for mounting. Following Reissner's approach, a stress function is introduced and two governing equations are derived in terms of the stress function and the axial deflection. Next, the surface deflections are evaluated from the calculated stress function and the axial deflection. As actuators, four lead-zirconate-titanate (PZT) thunder actuators are attached along the meridians separated by 90°, respectively. The forces developed by the actuators are expanded in a Fourier series and fed into the governing equations as boundary conditions at the outer edge. Finally, the deflection versus applied voltage is calculated analytically and its effect on the far-field radiation is given.**

***Index Terms*—Aperture antennas, mechanically adaptive antennas.**

NOMENCLATURE

E	Modulus of elasticity of the antenna shell.
G	Shear modulus of the antenna shell.
N_r	Stress resultant in the radial direction.
N_θ	Stress resultant in the circumferential direction.
$N_{r\theta}$	In-plane shear stress resultant.
n	Index for the terms in the Fourier expansion.
M_r	Moment couple on the surface perpendicular to the radial direction.
M_θ	Moment couple on the surface perpendicular to the circumferential direction.
$M_{r\theta}$	Twist moment couple.
P	Piezoelectrically induced force-per-unit length.
Q_r	Transverse shear resultant on the surface perpendicular to the radial direction.
Q_θ	Transverse shear resultant on the surface perpendicular to the circumferential direction.
R	Radius of curvature of the antenna.
r	Variable in the radial direction of the polar coordinate.
u_r	Displacement of a shell element in the radial direction.
u_θ	Displacement of a shell element in the circumferential direction.
a	Outer radius of the antenna aperture.
b:	Inner radius of the antenna aperture.
h	Thickness of the antenna shell.
q_r	Surface load in the radial direction.
q_θ	Surface load in the circumferential direction.
q	Surface load perpendicular to the surface.
w	Displacement of a shell element in the axial direction.
w_t	Width of a PZT actuator.
θ	Variable in the circumferential direction.
v	Poisson's ratio of the antenna shell.

Manuscript received October 15, 1998; revised December 16, 1999.

H.-S. Yoon and G. Washington are with the Intelligent Structures and Systems Laboratory, Department of Mechanical Engineering, The Ohio State University, Columbus, Ohio, 43210-1107 USA.

W. Theunissen is with the Department of Electrical Engineering, University of Pretoria, Pretoria, South Africa.

Publisher Item Identifier S 0018-926X(00)04385-4.

I. INTRODUCTION

SINCE the introduction of aperture antennas, the problem of dynamically varying the coverage area has been one of the main concerns of engineers in this area [1]. The development of reconfigurable reflectors and subreflectors represents a viable method of obtaining this goal [2], [3]. The performance of an antenna can be deteriorated by surface distortion of the antenna or by atmospheric disturbances caused by weather or environmental factors. In addition, beam steering leads to unwanted satellite reorientation. These deficiencies have led to the development of phased array antennas and adaptive electromagnetic structures [4]–[7]. Recently, as an alternative to the conventional antenna techniques, parabolic "singly curved" antennas that employ lead-zirconate-titanate (PZT) actuators have been studied by Washington [8] and Yoon [9]. Such antennas have the ability to change their shape by applying a voltage to the piezoelectric material that is bonded on the reflectors' surface. These antennas are capable of achieving beam steering and beam focusing.

In this paper, a "doubly curved" (bowl-shaped) adaptive aperture antenna utilizing PZT strips as actuators is studied. Some investigators have studied piezoelectric composite shells of various shapes where the piezoelectric material covers the whole area of the shell [10], [11]. In this study, however, the structure is modeled such that the piezoelectric actuators are strips that are bonded on small portions of the shell. The geometry of the antenna allows the use of Reissner's shallow shell theory [12]. The piezoelectric actuation is derived from externally applied forces along the outer edge of the actuators. With the calculated force applied as boundary conditions, the amount of deformation of the reflector surface is calculated analytically.

Finally, the far-field radiation pattern of the antenna is simulated from the deformed shape of the antenna.

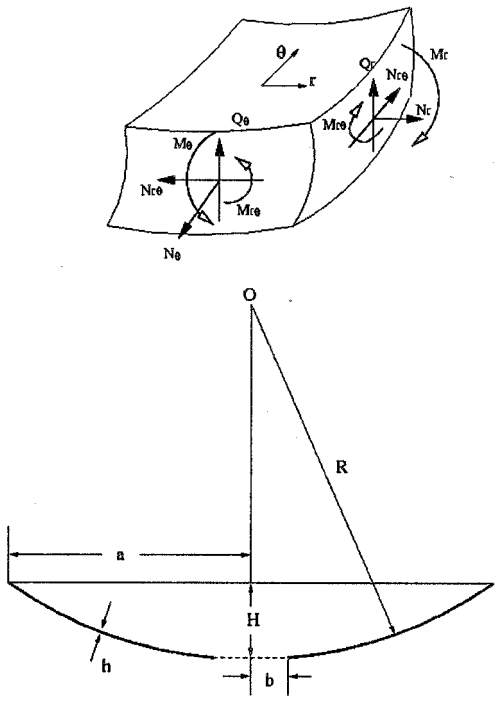

Fig. 1. Shallow spherical shell.

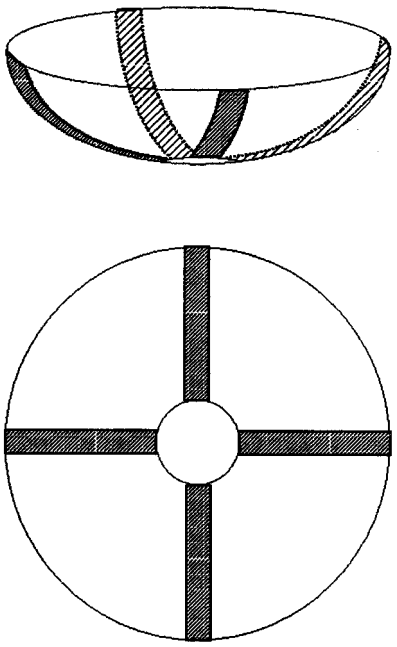

Fig. 2. Schematic of the spherical antenna with PZT actuators.

II. Shallow Spherical Thin Shells

The complete theory of shallow spherical thin shells can be found in the literature [12], [13]. A synopsis will be given here, for clarity, along with the more salient points relating to the active aperture system in question. The governing equations for a shallow spherical shell shown in Fig. 1 can be simplified as follows:

$$\frac{\partial(rN_r)}{\partial r}+\frac{\partial N_{r\theta}}{\partial\theta}-N_\theta+\frac{r}{R}Q_r+rq_r=0 \tag{1}$$

$$\frac{\partial(rN_{r\theta})}{\partial r}+\frac{\partial N_\theta}{\partial\theta}+N_{r\theta}+\frac{r}{R}Q_\theta+rq_\theta=0 \tag{2}$$

$$\frac{\partial(rQ_r)}{\partial r}+\frac{\partial Q_\theta}{\partial\theta}-\frac{r}{R}(N_r+N_\theta)+rq=0 \tag{3}$$

$$\frac{\partial(rM_r)}{\partial r}+\frac{\partial M_{r\theta}}{\partial\theta}-M_\theta-rQ_r=0 \tag{4}$$

$$\frac{\partial(rM_{r\theta})}{\partial r}+\frac{\partial M_\theta}{\partial\theta}+M_{r\theta}-rQ_\theta=0. \tag{5}$$

As was summarized by Kraus [13], neglecting the contributions of transverse shear stress resultants Q_r and Q_θ and omitting the external loads such as q_r, q_θ, and q reduce (1) and (2) to the following:

$$\frac{\partial(rN_r)}{\partial r}+\frac{\partial N_{r\theta}}{\partial\theta}-N_\theta=0 \tag{6}$$

$$\frac{\partial(rN_{r\theta})}{\partial r}+\frac{\partial N_\theta}{\partial\theta}+N_{r\theta}=0. \tag{7}$$

The above equations are satisfied if one introduces a stress function F by which the stress resultants are expressed as follows:

$$N_r=\frac{1}{r}\frac{\partial F}{\partial r}+\frac{1}{r^2}\frac{\partial^2F}{\partial\theta^2},\quad N_\theta=\frac{\partial^2F}{\partial r^2},$$
$$N_{r\theta}=-\frac{\partial}{\partial r}\left(\frac{1}{r}\frac{\partial F}{\partial\theta}\right). \tag{8}$$

It can be shown that the strain-displacement equation leads to the following compatibility equation:

$$\frac{1}{r^2}\frac{\partial^2\varepsilon_r^o}{\partial\theta^2}-\frac{1}{r}\frac{\partial\varepsilon_r^o}{\partial r}+\frac{1}{r^2}\frac{\partial}{\partial r}\left(r^2\frac{\partial\varepsilon_\theta}{\partial r}\right)$$
$$-\frac{1}{r^2}\frac{\partial^2(r\gamma_{r\theta}^o)}{\partial r\partial\theta}=\frac{\nabla^2w}{R} \tag{9}$$

where

$$\nabla^2=\frac{\partial^2}{\partial r^2}+\frac{1}{r}\frac{\partial}{\partial r}+\frac{1}{r^2}\frac{\partial^2}{\partial\theta^2}.$$

By substituting the following strain-stress equations

$$\varepsilon_r^o=\frac{1}{Eh}(N_r-\upsilon N_\theta) \tag{10}$$

$$\varepsilon_\theta^o=\frac{1}{Eh}(N_\theta-\upsilon N_r) \tag{11}$$

$$\gamma_{r\theta}^o=\frac{1}{Gh}N_{r\theta} \tag{12}$$

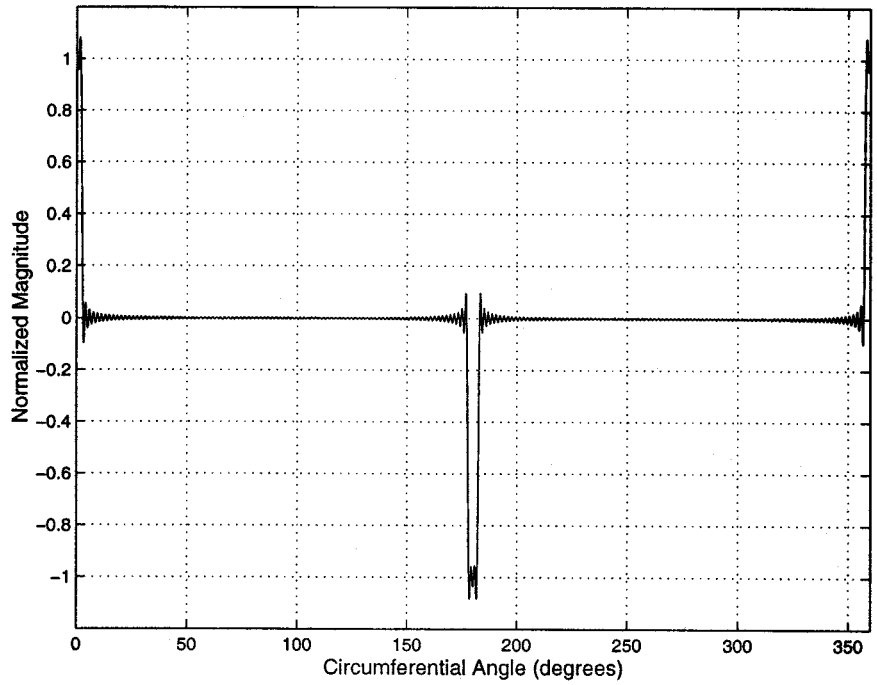

Fig. 3. First-mode actuation force expanded in Fourier series $(N = 100)$.

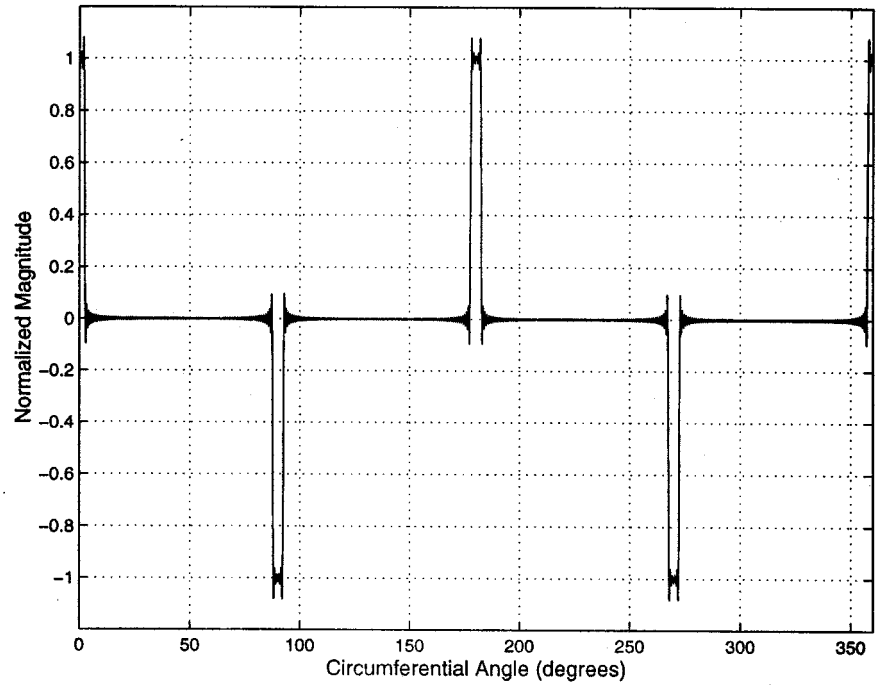

Fig. 4. Second-mode actuation force expanded in Fourier series $(N = 100)$.

into (9) and resorting to (8), one gets

$$\nabla^4 F - \frac{Eh}{R}\nabla^2 w = 0. \tag{13}$$

Note that (13) is an equation of the stress function F and the deflection in the axial direction w. Substituting Q_r and Q_θ from (4) and (5) into (3) results in

$$\frac{\partial}{\partial r}\left[\frac{\partial(rM_r)}{\partial r} + \frac{\partial M_{r\theta}}{\partial \theta} - M_\theta\right] + \frac{1}{r}\frac{\partial}{\partial \theta}\left[\frac{\partial(rM_{r\theta})}{\partial r} + \frac{\partial M_\theta}{\partial \theta} + M_{r\theta}\right] - \frac{r}{R}(N_r + N_\theta) = 0. \tag{14}$$

The shear resultants Q_r and Q_θ and moment couples M_r, M_θ, and $M_{r\theta}$ are written in terms of the curvature as follows:

$$Q_r = -D\frac{\partial \nabla^2 w}{\partial r} \tag{15}$$

$$Q_\theta = -D\frac{1}{r}\frac{\partial \nabla^2 w}{\partial \theta} \tag{16}$$

$$M_r = -D\left[\frac{\partial^2 w}{\partial r^2} + v\left(\frac{1}{r}\frac{\partial w}{\partial r} + \frac{1}{r^2}\frac{\partial^2 w}{\partial \theta^2}\right)\right] \tag{17}$$

$$M_\theta = -D\left[\frac{1}{r}\frac{\partial w}{\partial r} + \frac{1}{r^2}\frac{\partial^2 w}{\partial \theta^2} + +v\frac{\partial^2 w}{\partial r^2}\right] \tag{18}$$

$$M_{r\theta} = -D(1-v)\frac{\partial}{\partial r}\left(\frac{1}{r}\frac{\partial w}{\partial \theta}\right) \tag{19}$$

where

$$D \equiv \frac{Eh^3}{12(1-v^2)}.$$

Substituting these relations, which relate shear resultants and moment couples to the axial deflection into (14), results in

$$\nabla^4 w + \frac{1}{RD}\nabla^2 F = 0. \tag{20}$$

Therefore, the original five equations of force equilibrium have been reduced to two homogeneous equations of w and F. The two reduced governing equations, (13) and (20) can be rewritten as

$$w = \chi + \psi \quad \text{and} \tag{21a}$$

$$F = \phi - RD\nabla^2 \chi \tag{21b}$$

where χ, ψ, and ϕ satisfy the following equations:

$$\nabla^2 \psi = 0 \tag{22a}$$

$$\nabla^2 \phi = 0 \tag{22b}$$

$$\nabla^4 \chi + k_s^4 \chi = 0 \tag{22c}$$

where

$$k_s \equiv \left(\frac{12(1-v^2)}{R^2 h^2}\right)^{\frac{1}{4}} \tag{22d}$$

The general solutions for (22) are as follows:

$$\phi = A_{10} + A_{20}\log r + \sum_{n=1}^{\infty}(A_{1n}r^n + A_{2n}r^{-n})\cos(n\theta) \tag{23a}$$

$$\psi = B_{10} + B_{20}\log r + \sum_{n=1}^{\infty}(B_{1n}r^n + B_{2n}r^{-n})\cos(n\theta) \tag{23b}$$

$$\chi = \sum_{n=1}^{\infty}(C_{1n}\,\mathrm{ber}_n(k_s r) + C_{2n}\,\mathrm{bei}_n(k_s r) + C_{3n}\,\mathrm{ker}_n(k_s r) + C_{4n}\,\mathrm{kei}_n(k_s r))\cos(n\theta) \tag{23c}$$

where A's, B's, and C's are coefficients to be determined by applying boundary conditions. Finally, the radial and circumferential displacement u_r and u_θ can be written as

$$u_r = \frac{1}{R}\left(rw - \int \psi\, dr\right) - \frac{1}{2Gh}\frac{\partial F}{\partial r} + f(\theta) \tag{24}$$

$$u_\theta = r\int \frac{\partial}{\partial \theta}\left(\frac{\int \psi\, dr}{R}\right)\frac{dr}{r^2} - \frac{1}{2Gh}\frac{1}{r}\frac{\partial F}{\partial \theta} + f'(\theta) + g(\theta) \tag{25}$$

where $f(\theta)$ and $g(\theta)$ are arbitrary functions of integration. In analytical studies of mechanical systems, spherical structures are easier to model and analyze than their paraboloidal counterparts. In order to keep the analysis as simple as possible while simultaneously maintaining the accuracy associated with paraboloids, a geometric technique was used to find the family of spheres that best approximate paraboloids.

III. Modeling of the Antenna Surface

For the actuation of the antenna, four high deflection PZT thunder actuators are used. The antenna is a shallow spherical shell made of thin polymer called LEXAN, with a small circular portion around the apex cut out. Four actuators are bonded along the meridians separated by 90°, respectively, on the back surface of the antenna. The front surface of the antenna is painted with a thin layer of conductive paint to improve antenna performance. A schematic of the antenna is shown in Fig. 2. When the piezoelectric component of the actuator is energized by a positive or a negative voltage, its length expands or contracts, respectively. The expansion or contraction of the piezoelectric part introduces bending moments in the actuator and forces into the structure of the reflector. The actuators deform the reflector in a quasi-static manner meaning that the operating frequency is very low compared to the time constant of the mechanical system. Therefore, one does not need to consider any dynamics of the mechanical system. This also means that the reflector is not optimal for scanning. The effect of the piezoelectric actuation is modeled as external forces applied along the outer edge of the antenna in the direction perpendicular to the antenna surface. These forces push or pull the portions of the outer edge where the actuators are extended, thereby causing the antenna structure to deform in desired ways. Since there are four actuators, one can achieve various configurations of forces by applying different amounts of voltage to each actuator. To be able to apply the induced forces as boundary conditions of the governing equations of the antenna structure, it is necessary to express the forces in an analytical form such as Fourier series. In the current analysis, two different configurations of forces are used to generate two intended shapes of antenna. These configurations give some of the possibilities that can be achieved using the current configurations of the actuators. Other force configurations can be achieved by using different actuator configura-

TABLE I
PARAMETERS OF THE ANTENNA MODEL

Parameters	Value
Radius of the outer edge, a	0.3 (m)
Radius of the inner edge, b	0.01 (m)
Radius of curvature of antenna, R	1 (m)
Thickness of antenna shell, h	2.54×10^{-4} (m)
Width of actuator, w_t	0.0254 (m)
Thickness of Stainless Steel in actuator	2.03×10^{-4} (m)
Thickness of PZT in actuator	2.54×10^{-4} (m)
Piezoelectric constant, d_{31}	-190×10^{-12} (m)

tions. The force configurations in this study can be expressed in a Fourier series as the following:

$$Q_{r1}(\theta)=\sum_{n=1}^{\infty}\frac{2P}{(2n-1)\pi}\sin\left((2n-1)\frac{w_t}{2a}\right)\times(1-\cos(2n-1)\pi)\cos((2n-1)\theta) \tag{26a}$$

$$Q_{r2}(\theta)=\sum_{n=1}^{\infty}\frac{8P}{(4n-2)\pi}\sin\left((4n-2)\frac{w_t}{2a}\right)\cos((4n-2)\theta) \tag{26b}$$

where Q_{r1} and Q_{r2} are the shear stress resultants corresponding to the first and the second mode (beam steering and beam shaping) of the antenna respectively. In the above equations, w_t is the width of the actuators, a is the outer radius of the antenna, and P is the applied force per unit width. In this model, the applied force P is calculated based on the result of the actuation of a singly curved beam structure. In other words, applying the force P to a singly curved beam generates the same amount of tip deflection as will be seen when the beam is actuated by a PZT actuator bonded along the beam. The forces represented by (26) are shown in Figs. 3 and 4 when $P=1$. In Fig. 3, positive force is applied at $\theta=0^\circ$ and negative force is applied at $\theta=180^\circ$. This configuration of forces produces a steering movement in the antenna and the radiation pattern associated with this mode will show a shift in the main lobe. This mode is called the first mode or the beam steering mode. Fig. 4 shows that positive forces are applied at $\theta=0^\circ$ and $\theta=180^\circ$ and negative forces are applied at $\theta=90^\circ$ and $\theta=270^\circ$. The deformed antenna shape corresponding to this force configuration is defined as the second-mode shape. The radiation pattern for the second mode can be used for beam shaping. Beam shaping in this instance means widening or narrowing the main beam.

Since the lowest power in the Fourier series of the first-mode force is one, a special treatment for the mode is necessary as was outlined by Reissner [12]. When $n=1$, the two arbitrary functions $f(\theta)$ and $g(\theta)$ in (24) and (25) become multivalued in terms of the circumferential angle θ. This problem can be removed by introducing an additional stress function F^* of the form

$$F^*=A_0r(\theta\sin\theta-\log r\cos\theta) \tag{27}$$

to (21b). Once this is done, u_r, u_θ, and w for $n=1$ can be rewritten as the following:

$$u_r=\frac{1}{R}B_{11}\frac{r^2}{2}\cos\theta+\frac{1+v}{Eh}\left(2A_0\log r+\frac{A_{21}}{r^2}\right)\cos\theta+C_1\cos\theta+\frac{r}{R}\chi+\frac{1+v}{Eh}RD\frac{\partial}{\partial r}\nabla^2\chi \tag{28}$$

$$u_\theta=-\frac{1}{R}B_{11}\frac{r^2}{2}\sin\theta+\frac{1+v}{Eh}\left(-2A_0\log r+\frac{A_{21}}{r^2}\right)\sin\theta-C_1\sin\theta+\frac{1+v}{Eh}RD\frac{1}{r}\frac{\partial}{\partial\theta}\nabla^2\chi \tag{29}$$

$$w=\left(B_{11}r-\frac{1+v}{Eh}R\frac{A_0}{r}\right)\cos\theta+\chi \quad . \tag{30}$$

In the above equations, the following relation between B_{21} and A_0 was used to make $f(\theta)$ and $g(\theta)$ univalued:

$$\frac{1}{R}B_{21}+\frac{1+v}{Eh}A_0=0. \tag{31}$$

Like other cases, where $n\neq1$ [(28)–(30)] contain eight undetermined coefficients given by A_0, B_{11}, A_{21}, C_1, and the four C's from χ. For the terms corresponding to n's other than $n=1$, one has to resort to (21a)(21b) and (23). In (23), there are eight coefficients corresponding to every positive integer of n. When $n=0$, four coefficients exist. Since the four coefficients A_{10}, A_{20}, B_{10}, and B_{20} are not associated with θ, they are ignored in the current loading case where the applied forces are dependent on the circumferential angle θ.

The eight undetermined coefficients in (23) require eight boundary conditions. The boundary conditions for the first and the second mode of the antenna actuation are listed below.

At $r=a$ (outer edge)

$$N_r(a,\theta)=0 \tag{32a}$$

$$N_{r\theta}(a,\theta)=0 \tag{32b}$$

$$M_r(a,\theta)=0 \tag{32c}$$

$$Q_r(a,\theta)=Q_{r1}(\theta), \quad \text{for the first mode} \tag{32d}$$

$$=Q_{r2}(\theta), \quad \text{for the second mode.} \tag{32e}$$

At $r=b$ (inner edge)

$$u_r(b,\theta)=0 \tag{33a}$$

$$u_\theta(b,\theta)=0 \tag{33b}$$

$$w(b,\theta)=0 \tag{33c}$$

$$\frac{\partial w}{\partial r}(b,\theta)=0. \tag{33d}$$

Since the antenna is clamped along the inner edge, the boundary conditions at $r=b$ are zero deflection.

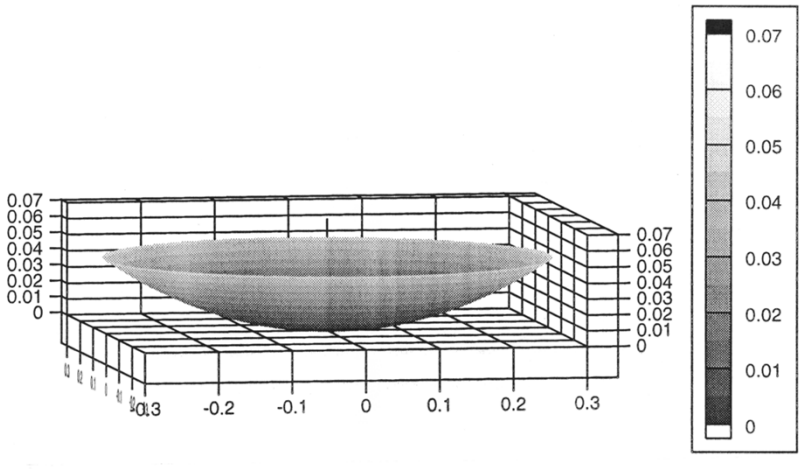

Fig. 5. Undeformed shape of antenna (all units in meters).

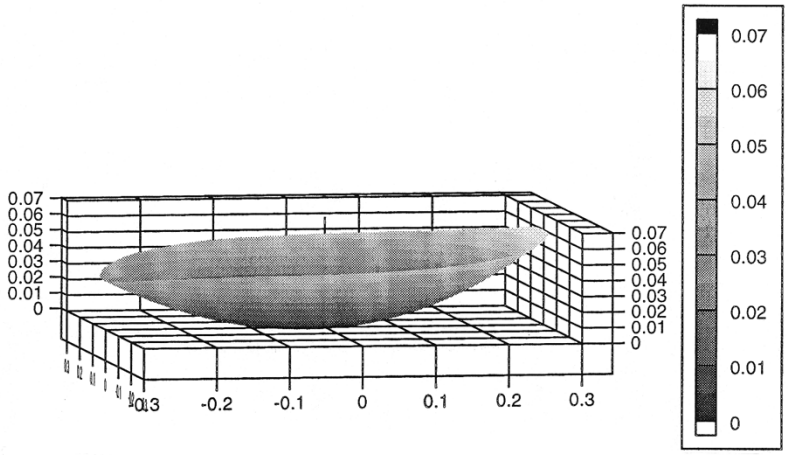

Fig. 6. Antenna shape in the first mode (all units in meters).

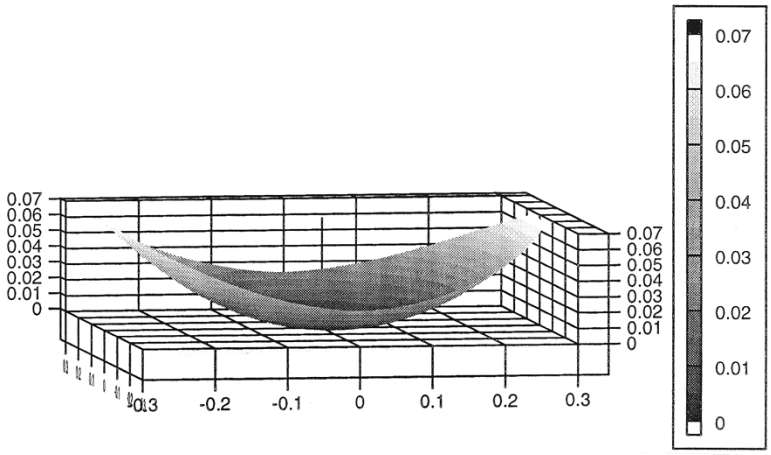

Fig. 7. Antenna shape in the second mode (all units in meters).

IV. Results

The deflections u_r, u_θ, and w were calculated for the two modes. The parameters used for calculating the deflections are listed in Table I. The undeflected shape of the antenna surface is shown in Fig. 5, where all dimensions are in meters. Using the results of (21)–(22), the first and the second mode shapes of the antenna are plotted in Figs. 6 and 7. For the two actuated shapes

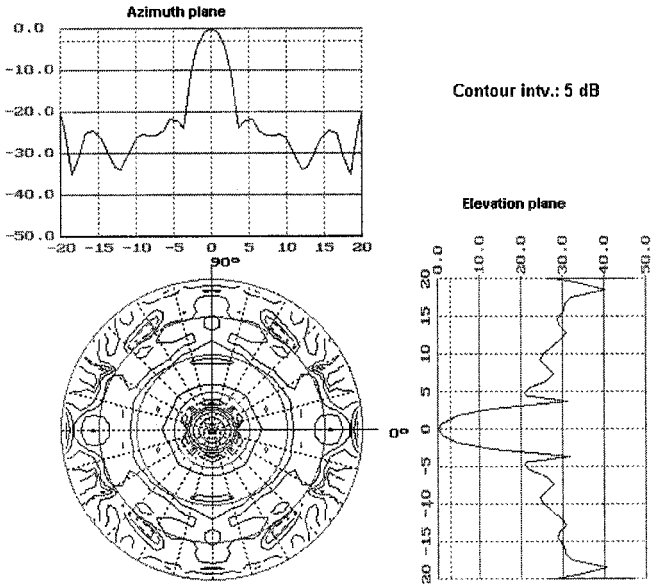

Fig. 8. Simulated radiation pattern of the undeformed antenna.

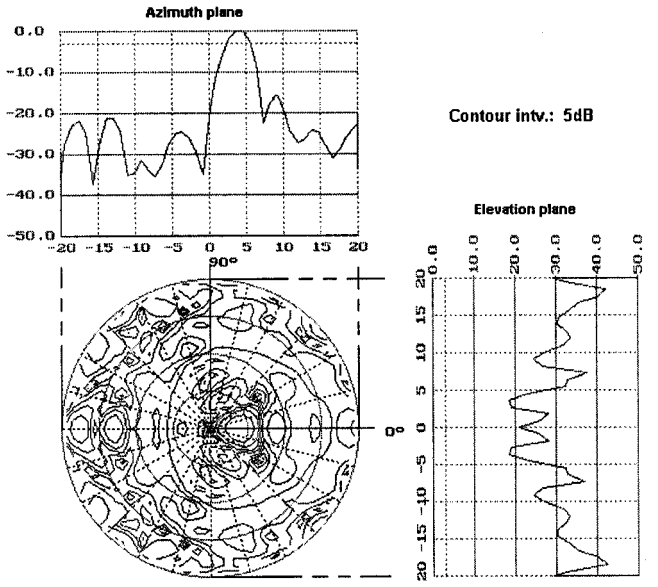

Fig. 9. Simulated radiation pattern of the first mode shape $(V = 300)$.

of the antenna, the far-field radiation pattern was simulated with respect to the applied voltage and is shown in Figs. 8–12. The far-field radiation is calculated using the methodology developed by Rahmat-Samii and Galindo-Israel [14]. The induced physical optics current on the reflector is given by

$$\vec{J} = 2\hat{n} \times \vec{H}_s(\vec{r}_s') \tag{34}$$

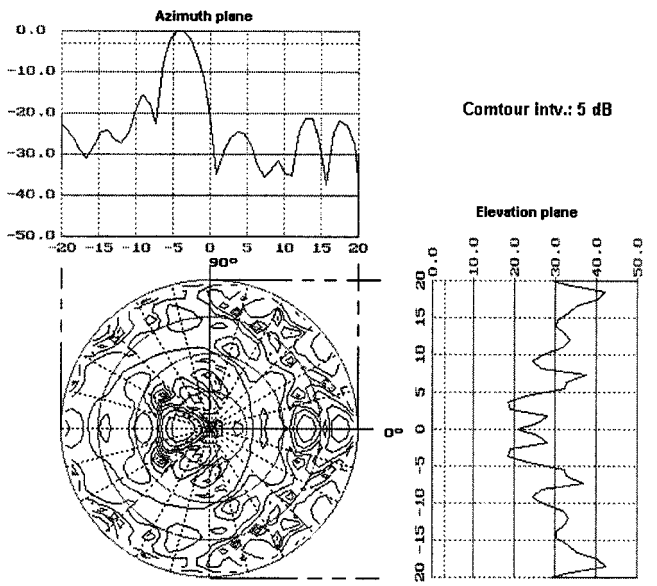

Fig. 10. Simulated radiation pattern of the first mode shape $(V = -300)$.

where $\hat{n}$ is a unit normal vector to the reflector surface and $\vec{r}_s'$ is a position vector of the reflector. By the far-field approximation $|\vec{r} - \vec{r}_s'| \approx \vec{r} - \vec{r} \cdot \vec{r}_s'$, the magnetic intensity vector $\vec{H}$ and the electric field intensity vector $\vec{E}$ can be represented as follows:

$$\vec{H} = jk\frac{e^{-jkR}}{4\pi R}(T_\phi\hat{\theta} - T_\theta\hat{\phi}) \tag{35}$$

$$\vec{E} = jk\eta\frac{e^{-jkR}}{4\pi R}(T_\theta\hat{\theta} - T_\phi\hat{\phi}) \tag{36}$$

where

$$\vec{T} = \iint_S \vec{J}(\vec{r})e^{jk\vec{R}\cdot\hat{r}}\,dS.$$

In Fig. 8, the radiation pattern for the undeformed antenna shape is plotted. It shows the main lobe at the center and several side lobes around it. Figs. 9 and 10 show the radiation pattern for the first mode actuated by 300 V and −300 V, respectively. One can see that the main lobe and side lobes steer according to the polarity of the applied voltage. Figs. 11and 12 show a flattening and widening of the main lobe. As expected, the first mode shows beam steering and the second mode shows beam shaping.

V. Conclusions and Future Work

The work in this study outlines the methodology for the next generation of reflector antennas. In order to accomplish this, a doubly curved piezoelectrically actuated aperture antenna was modeled and analyzed. The deflections of the structure were calculated using shell theory augmented with piezoceramic elements. The far-field radiation was calculated using physical optics techniques. This study shows that an active aperture antenna can be developed and used to change far-field radiation patterns by shape changing. It has been known for quite some time that the effects on the far-field radiation shown in this study

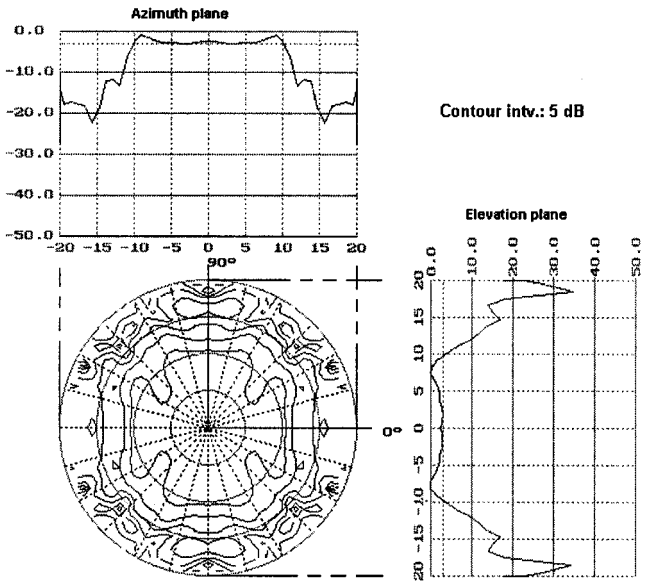

Fig. 11. Simulated radiation pattern of the second mode shape $(V = 300)$.

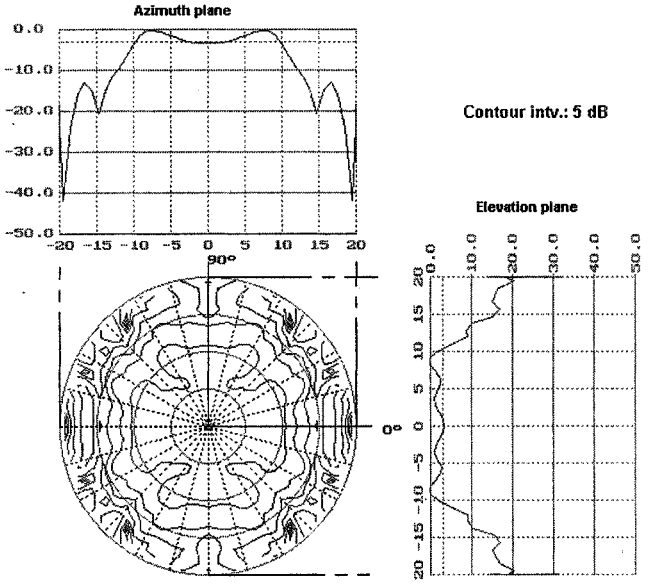

Fig. 12. Simulated radiation pattern of the second mode shape $(V = -300)$.

can be achieved by moving the feed with a rigid reflector. However, there are a myriad of shapes that one can achieve in this formulation that cannot be achieved by feed point variation. These shapes stem from the application of different combinations of voltages to the actuators. In addition, extra actuators can be added to give even more shape possibilities. An additional caveat of this formulation stems from the capacitive nature of the actuators. The actuators use high voltages but consume very little current. This means that the overall power consumption needed to make a control move is small.

Future work in this area will consist of a working prototype whose performance will be tested experimentally. The data acquired from the field test will be compared to the one analytically calculated in this paper. Also, a control unit, which will calculate and apply voltages to each actuator, will be developed and tested.

REFERENCES

[1] L. Silverberg and G. Washington, "Modal control of a corner reflector to maximize far-field power," *Microwave Opt. Technol. Lett.*, vol. 8, no. 5, pp. 260–264, 1995.
[2] P. R. Lawson and Y. L. Yen, "A piecewise deformable subreflector for compensation of cassegrain main reflector errors," *IEEE Trans. Antennas Propagat.*, vol. 36, pp. 1342–1350, Oct. 1988.
[3] P. J. B. Clarricoats, A. D. Monk, and H. Zhou, "Array-fed reconfigurable reflector for spacecraft systems," *Electron. Lett.*, vol. 30, no. 8, pp. 613–614, 1994.
[4] W. L. Stutzman and G. A. Thiele, *Antenna Theory and Design*. New York: Wiley, 1981.
[5] P. W. Howells *et al.*, "Special issue on adaptive antennas," *IEEE Trans. Antennas Propagat.*, vol. AP-24, pp. 575–764, Sept. 1976.
[6] B. M. Howard and N. E. Tornberg, "Thermoadaptive and electroadaptive antennas for smart skin applications," in *Panel 3 Phys. Electron. Workshop Smart Electromagn. Antenna Structures*, Nov. 1996.
[7] T. M. Au and K. M. Luk, "Effect of parasitic element on the characteristics of microstrip antennas," *IEEE Trans. Antennas Propagat.*, vol. 39, pp. 1244–1251, Aug. 1991.
[8] G. Washington, "Smart aperture antennas," *Smart Mater. Structure*, vol. 5, pp. 801–805, 1996.
[9] H.-S. Yoon and G. Washington, "Piezoceramic actuated antennas," *Proc. SPIE Conf. Smart Structures Intell. Syst.*, vol. 3328, pp. 156–163, 1998.
[10] H. S. Tzou, *Piezoelectric Shells: Distributed Sensing and Control of Continua*. Boston, MA: Kluwer, 1992.
[11] P. H. Larson, "The use of piezoelectric materials in creating adaptive shell structures," Ph.D. dissertation, Univ. Delaware, Newark, DE, 1994.
[12] E. Reissner, "On the determination of stresses and displacements for unsymmetrical deformation of shallow spherical shells," *J. Math. Phys.*, vol. 38, pp. 16–35, 1959.
[13] H. Kraus, *Thin Elastic Shells*. New York: Wiley, 1967.
[14] Y. Rahmat-Samii and V. Galindo-Israel, "Shaped reflector analysis using the Jacobi-Bessel series," *IEEE Trans. Antennas Propagat.*, vol. AP-28, pp. 425–435, July 1980.

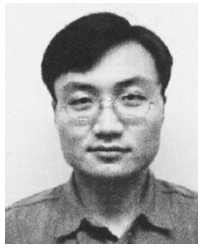

Hwan-Sik Yoon received the B.S. degree (*cum laude*) in physics education from Seoul National University, Seoul, Korea, in 1994, and the M.S. degree in mechanical engineering from The Ohio State University, Columbus, in 1998. He is currently working toward the Ph.D. degree in the Intelligent Structures and Systems Laboratory, Mechanical Engineering Department, The Ohio State University.

He is currently developing smart aperture antenna systems for use in space-borne applications. His research includes modeling and control of intelligent structures.

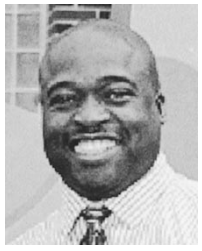

Gregory Washington received the B.S. *(magna cum laude)*, M.S., and Ph.D. degrees, all in mechanical and aerospace engineering, from North Carolina State University, Raleigh, in 1989, 1991, and 1994, respectively.

In 1995, he joined the Mechanical Engineering Department, The Ohio State University, Columbus, where he is currently an Assistant Professor. He has published over 30 journal and conference articles related to smart materials and the control of mechatronic systems. His areas of interest include modeling and control of smart materials, intelligent control, and modeling can control of mechatronic systems.

Dr. Washington was the recipient of a National Science Foundation CAREER Award in 1997.

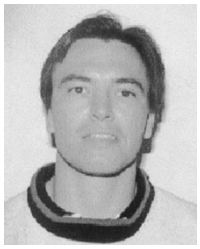

Wilhelmus Hendrikus Theunissen was born in South Africa in 1966. He received the B.Eng. and M.Eng. (*cum laude*) degrees in electronic engineering from the University of Stellenbosch, Stellenbosch, South Africa, in 1988 and 1990, respectively, and the Ph.D. degree in electronic engineering from the University of Pretoria, Pretoria, South Africa, in 1999.

He is currently a Senior Research Associate at the ElectroScience Laboratory, The Ohio State University, Columbus. His research interests include antenna and RCS measurement software development, shaped contour beam reconfiguration techniques for reflector antennas, and antenna development.